Polymer Testing 113 (2022) 107655

Contents lists available at ScienceDirect

Polymer Testing

journal homepage: www.elsevier.com/locate/polytest

Elastomer-based skins for morphing aircraft applications: Effect of biaxial strain rates and prestretch

Dilshad Ahmad [a,*], Rafic M. Ajaj [a], Mohammadreza Amoozgar [b]

[a] Department of Aerospace Engineering, Khalifa University, Abu dhabi, United Arab Emirates
[b] Department of Mechanical, Materials and Manufacturing Engineering, University of Nottingham, NG7 2RD, UK

ARTICLE INFO

Keywords:
Polymers
Biaxial characterization
Prestretch
Morphing wing
Ecoflex
DIC

ABSTRACT

There is an emerging trend in the morphing aircraft research where two or more morphing degrees of freedom are used on a wing which leads to the concept of polymorphing. The skin of the morphing wing must be flexible in the morphing direction but stiff in other directions to withstand the aerodynamic loads and maintain the airfoil shape. Polymorphing changes the loadings profile (from uniaxial to biaxial) and increases the complexity of designing suitable morphing skins. Furthermore, elastomeric materials used on morphing wings are usually prestretched to prevent wrinkling and to increase their out-of-plane stiffness. This paper focuses on elastomeric morphing skins and it studies the effect of biaxial strain rates and prestretch ratios on important mechanical properties such as stiffness, hysteresis losses (%), and stress relaxations (%) from an experimental perspective. Three polymeric materials are considered: Latex, Oppo, and Ecoflex. This study provides a mechanical comparative understanding of the three polymers used in the morphing wing under biaxial loading (two morphing degrees of freedom).

1. Introduction

A major aim of aerospace industries is to develop aircraft with better efficiency than that of their predecessors [1–3]. To this end, aerospace industries are focusing on optimizing the aerodynamic and structural layouts of aircraft [4–6]. To achieve this, the concept of morphing wings has been implemented recently in air vehicles. This is because existing aircraft wings with hinged ailerons or flaps connections that account for sudden changes in the cross-section cause aerodynamic losses with excessive noise and vibration in the airframe [7,8]. The morphing wing is a potential solution to these drawbacks as it could change its shape and size without opening gaps in and between itself and it operates smoothly as a single entity with a smaller actuation force requirement [9–12].

The most important part in the pursuit of a lightweight morphing wing is the flexible skin that covers ribs and morphing structures underlying beneath it [13]. The foremost requirement for a morphing flexible skin is its two ways seamless change in shape [5]: Firstly, lengthwise change in surface area (span, flaps, slats in wing) and secondly, chordwise changes in surface area (camber, aileron, winglets, and pitch propeller in airplane wing). Recently, a new trend in the morphing aircraft research, wherein two or more morphing degrees of freedom are implemented on a wing leads to the concept of polymorphing. Polymorphing changes the loadings profile (from uniaxial to biaxial) and increases the complexity to design suitable morphing skins. Also, for polymorphing wings (for example, span and camber morphing), the deformation of stretched polymeric skin mimics the biaxial deformation mode. Here, a biaxial mode can be defined as stretching the skin with 2 degrees of freedom along transverse axes (X and Y) with different actuation rates. Following this, one of the most promising compliant skin morphing concepts utilizes flexible/elastomeric materials which are both flexible and restrained to aerodynamic loads [14,15]. For example, Kikuta et al. [16] investigated different kinds of materials to be applied in the morphing wings. They tested polyurethanes, copolyesters, shape-memory materials, and woven materials. They investigated that the mechanical properties of polyurethanes like Tecoflex 80 A are well suited to be implemented in morphing wings. Kuduva [17] then investigated silicone-based polymer as a candidate material for morphing wing. Their experimental work revealed that the silicone-based material for morphing wings improves the aerodynamic performance of military aircraft. In a series of works, Olympio and Gandhi [18,19] focused on the elastomeric materials applied in the morphing wings. They implemented elastomeric sheets with cellular substructure and curved strands. Their studies suggested that the use of flexible skin reduces the actuation force appreciably. In a similar work, Olympio and Gandhi [20] proposed a zero Poisson's ratio honeycomb structure with a flexible skin. Consequently, it substantially reduced the effective

* Corresponding author.
E-mail addresses: dilshad.ahmad@ku.ac.ae (D. Ahmad), rafic.ajaj@ku.ac.ae (R.M. Ajaj), M.Amoozgar@nottingham.ac.uk (M. Amoozgar).

https://doi.org/10.1016/j.polymertesting.2022.107655
Received 12 March 2022; Received in revised form 25 May 2022; Accepted 31 May 2022
Available online 6 June 2022

stiffness of the polymeric skin in the non-morphing direction. Bubert et al. [21] synthesized an elastomeric sheet for span morphing. Their results showed that a 100% increase in surface area of elastomeric skin is achieved when 100% span extension took place with almost zero Poisson's ratio. Ajaj et al. [11] applied a flexible latex skin in the zigzag wingbox concept. This soft skin allowed a maximum of 44% one-dimensional span extension. Woods and Friswell [22] developed a zero Poisson's ratio elastomeric skin and implemented it in the wing after prestretching. They observed an increase in actuation force of the morphing wing with the increase in prestretch values. Parancheerivilakkathil et al. [13] developed a novel polymorphing wing capable of 10% span extension while 20% camber change. Therein, they applied prestretched latex skin to avoid wrinkle formation during camber morphing. Their results suggested that the wrinkles can be completely avoided with a 15% prestretch of the latex skin. Also, Ajaj et al. [14] developed a polymorphing wing for small UAVs named Active Span morphing And Passive Pitching using a prestretched latex sheet. Their findings revealed that up to 25% span extension is required to increase aerodynamic efficiency. At the same time, passive pitching was used for alleviating gust loads. Recently, Kolbl and Ermanni [23] developed a novel polymer-based layered morphing skin and applied it to a camber morphing for small aircraft. The skin developed is a load-carrying skin that can undergo two-dimensional planar strains. In their deformation analysis, the biaxial straining of 10% and 16% is achieved in the span and chord direction, respectively.

Above literature studies suggests that different polymer-based materials have been used in morphing wings because of their extreme stretchability, low in-plane, and high out-of-plane stiffness [9,12]. In general, high out-of-plane stiffness of the polymeric material is achieved by prestretching before applying to the morphing wings [24,25]. However, due to the viscoelastic nature of the polymeric materials, they show pronounced dissipative losses and strong rate dependencies [26]. Especially, for a polymorphing wing utilizing prestretched polymeric materials, their characterization in biaxial ways (2 degrees of freedom) is considered a complicated task [22,27,28]. However, to pave the way for modeling morphing structures, it is essential to characterize the polymeric material in biaxial mode considering the effect of prestretch. Researchers have characterized the polymeric material but most of the works are limited to uniaxial mode only [29,30]. For example, Sahu and Patra studied the effect of strain rate on the viscoelastic losses in the uniaxial mode of a soft polymer, VHB [31]. Their results showed an increase in the hysteresis losses with the increase in strain rate. Hossain et al. [32] conducted uniaxial mechanical tests like loading–unloading and stress relaxation on VHB. They used Bergstrom Boyce's viscoelastic model to fit the experimental data and they established that both are in good agreement. Also, Kaltseis et al. [33] conducted a series of uniaxial experiments on three different polymers, Oppo 8003, ZruElast A1040, and VHB. They found that the Oppo has the least hysteresis loss. In addition, very few researchers have characterized the polymeric material in the biaxial loading mode. Helal et al. [34] conducted loading–unloading tests on VHB and finally proposed a model to predict the dissipation energy of polymers. Their model fits the experimental data with good agreement. Ahmad et al. [35] conducted a test using prestretched VHB. They simulated the stress–strain test by incorporating different lateral prestretch values in a pure shear fixture. Their findings revealed that the stiffness decreases with the increase in prestretch. In another work, Ahmad et al. [36] compared stress–strain curves under uniaxial, pure shear, and equibiaxial modes of deformation for VHB and Ecoflex material. They also compared the fracture behavior of the polymers under biaxial and equibiaxial modes. Also, Johlitz and Debels [37] presented the uniaxial and biaxial characterization of silicone polymers and their data are fitted to the standard material model. It is concluded that the uniaxial pull data can be fitted only up to small strains but cannot be fitted for the equibiaxial mode of deformation. More recently, Ahmad and Ajaj. [38] carried out multiaxial deformation tests including uniaxial, pure shear, biaxial and equibiaxial tests on Latex at a constant strain rate. Their findings revealed that the stiffness in the biaxial transverse direction is maximum among other modes of deformation.

Although literature studies have shown that the polymeric materials are characterized under uniaxial, pure shear and equibiaxial modes, but their extensive characterization in the biaxial deformation mode under different strain rates for various materials is absent. It should be noted that from a modeling perspective, it will give erroneous result when the mechanical properties obtained from one mode is applied to model the morphing wing deforming in other modes like biaxial [35,37]. Furthermore, despite using prestretched polymers for morphing wing applications, their biaxial mechanical characterization is not reported till now. Hence, the current contribution fills an important research gap of comparative biaxial experimental characterization of three different polymeric materials. The current contribution is the first of its kind of biaxial mechanical comparative study of polymers for various strain rates and prestretch values. To this end, the effect of strain rates on the mechanical properties under the biaxial mode of deformation is conducted for the three polymers: Latex, Oppo, and Ecoflex. In addition, the effect of pre-stretched skin on the stiffnesses, hysteresis (%), and stress relaxations (%) are also compared for the three polymers.

2. Experimental procedures

2.1. Experimental set up and conditions

The equipment (Model: Biotester 5000, Make: CellScale) used for testing three polymers in the biaxial mode of deformation is shown in Fig. 1. It consists of 13 major parts as shown in Fig. 1(a) and (b). A CCD camera is attached to the camera stand to measure the strains developed in the specimen when the deformation takes place in the biaxial modes. To capture a clear image, the device is equipped with two lamps. Four stepper motors are attached at the four corners of the device. Four magnetic grippers are attached with the stepper motors through four goosenecks. The magnetic side of the gripper is attached with the goosenecks while the other side is used to hold the specimen. To hold the specimen, five tungsten-made tines at a spacing of 1 mm are pierced into the polymeric specimen from all four sides. To insert the tines into the specimen, a long specimen holder called 'mounting bridge' having a square shape red colored backing material in the middle is used. A square specimen is kept on the backing material and the stage is raised using a fluid chamber. Then, all the 20 tines are gently pressed into the specimen from the four sides using a pressing block. The tines are gently removed from the backing material by partially lowering the stage using a lifting handle. Finally, the mounting bridge is removed to run the test. A simple USB interface is available for easy connection to the host computer to collect real-time data and pictures in the LabJoy software. The resolution of the image obtained is 1280 pixels × 960 pixels and the camera captures an image at a rate of 15 frames per second. The force required to stretch the material is measured by the 5N load cells. The load cells are protected from mechanical overloading with semiconductor strain gauge-based features. When the material is stretched, all the actuators are driven by four stepper motors. Each motor can be independently operated with a maximum velocity of 5 mm/s. Before running each test, the load cells are reset to zero values in the software. In the current contribution, all the results are explained in terms of engineering stress (MPa) and engineering strain (%). Engineering stress is calculated by dividing the force data divided by the initial cross-sectional area of the specimen. The cross-sectional area of the specimen is obtained by multiplying the width and thickness of the specimen before loading starts. All the tests are conducted at a room temperature of 22 °C. Generally, morphing wings with elastomeric skin in small unmanned aerial vehicles (UAVs) encounter uniform temperature because of their flight at very low altitudes [12]. Therefore, the effect of temperature on the polymers is not studied in the current contribution similar to the work of Li et al. [39] and Liao et al. [40].

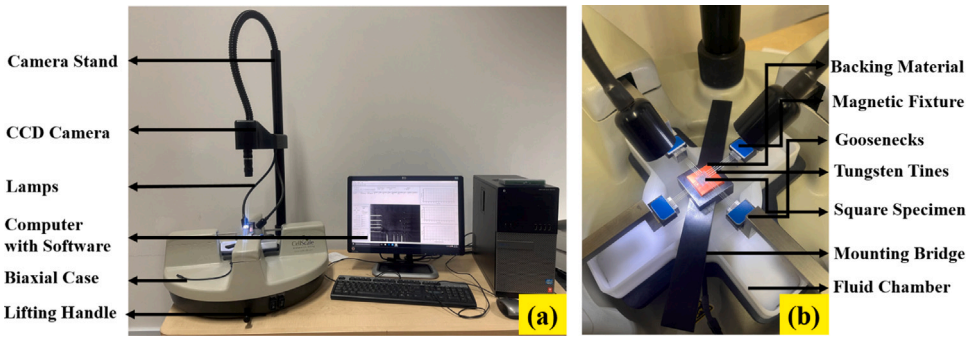

Fig. 1. (a) Biaxial device used for testing Latex, Oppo and Ecoflex under biaxial deformation modes. (b) Enlarged view showing how to mount the specimen.

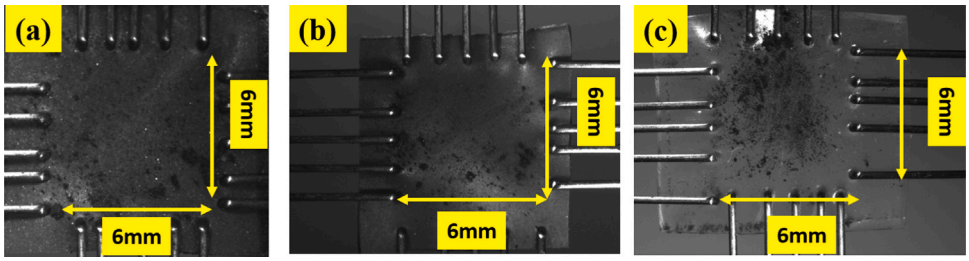

Fig. 2. Geometry of the specimen for (a) Latex (b) Oppo and (c) Ecoflex mounted on Biaxial Testing Machine.

2.2. Specimen geometry, materials and material synthesis

The geometries of the specimen for Latex, Oppo band (called Oppo), and Ecoflex are given in detail in Fig. 2. A 7 mm × 7 mm sized square sample is cut from the sheets of the polymeric materials and attached to the fixture to get a grip to a grip distance of 6 mm from both sides. This size of the specimen is selected due to the limitation of the machine stroke limit. The most commonly used polymeric material in aerospace applications is Latex [13]. Latex is from the family of natural rubber and is commercially available from Radical Rubber [41]. The thickness of the Latex sheet is selected as 0.25 mm. Another natural rubber-based polymer, Oppo which is used in physiotherapy for medical purposes is selected to test for the morphing wing application. This material is chosen knowing the fact that it is already durable because it is used for exercise purposes where it undergoes cyclic deformation many times. Earlier, Oppo was used for energy harvesting purposes as a dielectric elastomer [33]. It is purchased from Oppo Medical Inc. and its thickness is 0.25 mm [42]. Another silicone-based polymer, Ecoflex is selected to test for the purpose and is purchased from Smooth-ON, USA [43]. This material is selected because silicone-based polymers have been used in morphing wing applications. It comes with different shore hardness like Shore 00–10, Shore 00–20 Shore 00–30, and Shore 00–50. We have selected Ecoflex 00–50 having highest shore hardness to carry out a test for the current purpose. The material is considered soft and has a reasonable curing time and pot life of 4 h and 18 min, respectively. This makes Ecoflex easy to be synthesized in the laboratory.

To synthesize the silicone polymer, part A and part B of Ecoflex 00–50 (platinum cured) are first mixed by equal weight. Then, the mixture is mixed properly by stirring continuously for 3-4 min and is poured on a flat acrylic plate as shown in Fig. 3. Furthermore, a 300 mm wide Micrometer Adjustable Film Applicator (Model: SH 3042, Make: TQC Sheen) is used to make a sheet of uniform thickness. The two micrometers on the head of the applicator are first fixed at 0.5 mm and then the applicator is moved over the mixture for 3–4 strokes. It brings down the excess mixture coming out from the flat plate. The remaining dispersed mixture is then cured at room temperature for about 4 h. The thickness of the prepared sheet is then measured with the help of a portable thickness gauge (Model: Yunir1z5xbr97ut, Make: Yunir) as shown in Fig. 3(b). The caliper has a measuring range of 0–12.7 mm with an accuracy of 0.01 mm. The LCD digital display is clear for reading. To confirm, thickness is measured from at least five different parts of the sheet as shown in Fig. 3(b). The thickness is found to be in the range of 50 mm ± 0.04 μm. The sheet is then ready to be used for mechanical testing in the biaxial device as shown in Fig. 1.

2.3. Different biaxial strain rate conditions

There are majorly three different biaxial strain rate conditions applied in the current work and their respective strain maps at different times are shown in Fig. 4. In case 1, the strain rates in the X- direction is fixed at 2.3%/s while the strain rates in the Y direction is varied as 0.37%/s, 0.73%/s and 1.50%/s, respectively. The strain maps at a biaxial strain rate at X-2.3%/s, Y-0.73%/s are shown in Fig. 4(i). The representation of strain maps at $t = 0$ and $t = 50$ s are shown for Latex, Oppo, and Ecoflex, respectively. The strains at $t = 0$ s and $t = 50$ s are around 0% and 117% for X direction, while it is 0% and 40%, respectively for all the materials as shown in Fig. 4(i) (a), (b), (c) and (d).

In the second condition called case 2, we keep the X directional strain rate double the strain rate in the Y direction. This case is applicable for polymorphing skin encounters with different actuation speeds in the biaxial direction. While keeping the above-mentioned ratio of the strain rate the same, the magnitude of strain rates in the X direction varies as 11.75%/s, 4.7%/s, and 1.1%/s while, the respective strain rates in the Y directions are 5.75%/s, 2.37%/s and 0.5%/s. In this particular case, the representation of biaxial strain maps is shown for the three materials at the initial and final positions of loading. A strain rate of X-4.7%/s, Y-2.3%/s is selected to represent it as shown in Fig. 4 (ii). The strains at $t = 0$ s and $t = 25$ s are around 0% and 57%, respectively for all the materials as shown in Fig. 4 (ii) (a), (b), (c) and (d).

In the third condition, called case 3, we keep the strain rates in both the X and Y directions the same. This is a special case of biaxial loading called the equibiaxial mode of deformation. While keeping the strain rates equal in both the X and Y directions, the magnitude of strain rates changes to 4.7%/s, 1.1%/s, and 0.78%/s, respectively. In this particular case, the representation of equibiaxial strain maps is shown for the three materials at the initial and final positions of

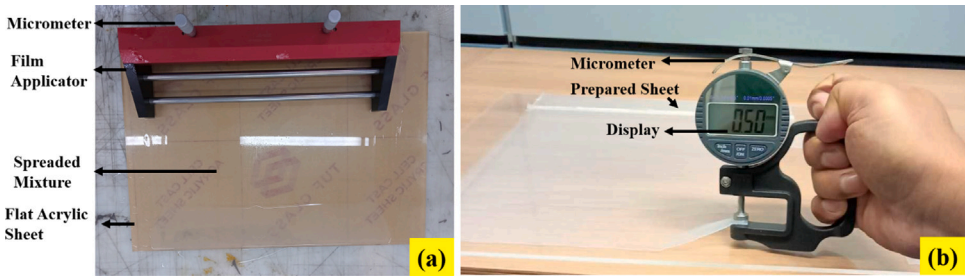

Fig. 3. Synthesis of Ecoflex 00–50 sheets with the help of (a) film applicator and (b) measurement of thickness with the help of portable thickness gauge.

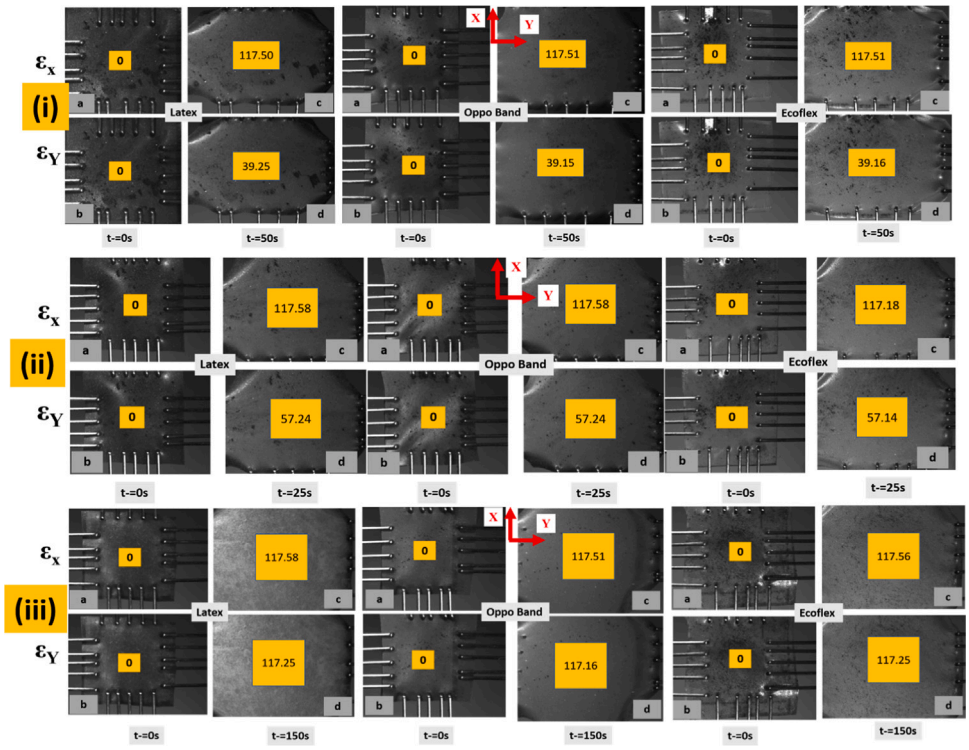

Fig. 4. Representation of biaxial strains for case 1 developed in the X and Y directions for Latex, Oppo and Ecoflex at a fixed strain rate of X-2.3%/s, Y-0.73%/s at different times. (ii) Representation of biaxial strains for case 2 (different strain rates in the Y direction) in the X and Y directions at a strain rate of X- 4.7%/s, Y-2.3%/s at different times. (iii) Representation of equibiaxial strains for case 3 in the X and Y directions at a strain rate of X-4.7%/s, Y-4.7%/s for different times.

loading. A strain rate of X-4.7%/s, Y-4.7%/s is chosen to represent it as shown in Fig. 4 (iii). The strains at $t = 0$ s and $t = 150$ s are around 0% and 117%, respectively for all the materials as shown in Fig. 4 (iii) (a), (b), (c) and (d). Small unmanned aerial vehicles (UAVs) fly at very low altitude level and the morphing of wing generally takes place for very little time during its flight depending upon the types of morphing [12,44]. Therefore, we have selected a range of times varying between a minimum of 10 s and a maximum of 150 s for the biaxial stretching of the specimen. Hence, for 117% stretching for a period of 10 s in the biaxial machine, the strain rate is 11.7%/s which is the highest strain rate similar to work done by Liao et al. [45]. A maximum stretch of 117% (for strain rate case) and 280% (for prestretch case) are selected to avoid nonuniformity in the specimen due to gripping from the tines. This is termed a fast strain rate in the current study that corresponds to the camber morphing. On the other hand, for span morphing, the skin deforms for more time [46]. Therefore, for stretching of 117% in a period of 150 s, the strain rate is 0.78%/s. Hence, as per the practical perspective of morphing wing, we have tested all the specimens below a strain rate of 11.7%/s following earlier works [33,38].

2.4. Different prestretch conditions

In the current contribution, three different prestretch conditions are employed as shown in Fig. 5. In the first kind of prestretching, the specimen is prestretched up to a particular strain in the Y direction and then loading is applied in both the X and Y directions as shown in Fig. 5(i). In the second type of prestretching, the specimen is pre-stretched in the Y direction and loading is applied in the X-direction keeping the Y direction constrained as shown in Figure (ii). In the third case, the specimen is prestretched in the Y direction and then loading is applied in the same direction as shown in Fig. 4 (iii). In each case discussed above, the specimen after prestretching is kept for stress relaxation for around 480 s and then further loading is applied following the earlier work [38,47]. From a simulation and modeling perspective, the relaxation time for polymers is around 1hr [48,49].

2.5. Digital image correlation (DIC) technique in the biaxial testing machine

The biaxial testing machine has an integrated image analysis software used to measure strains through the DIC technique. This can be accessed by selecting the 'Analyze and Review Images' section from the

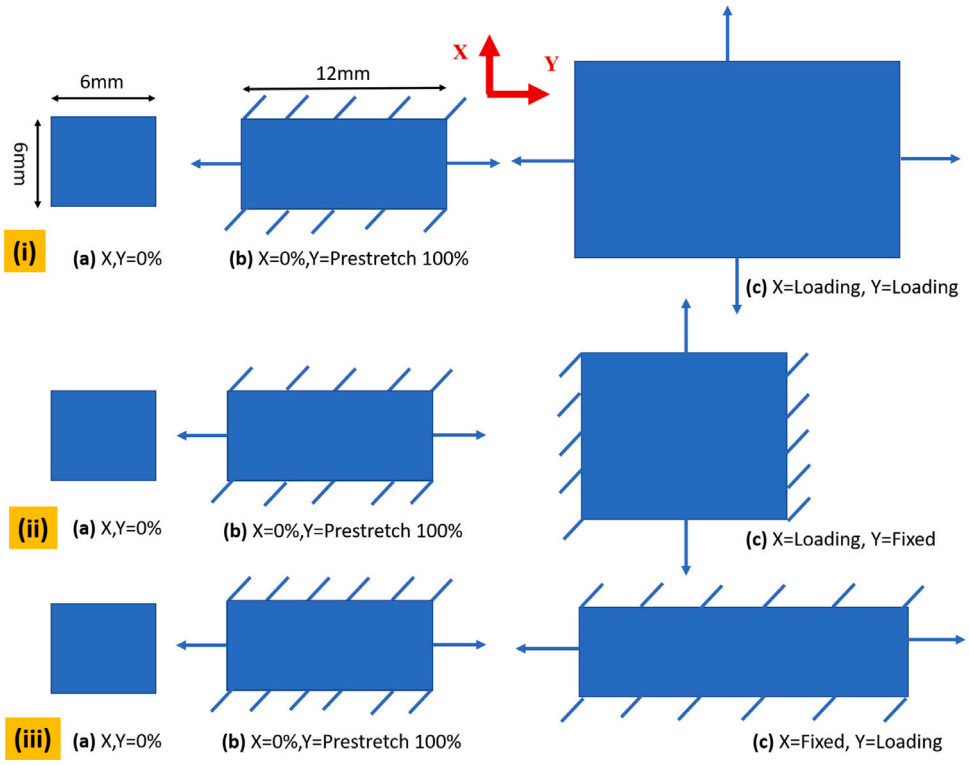

Fig. 5. Representation of three different prestretch conditions as (i) prestretching the specimen in the Y direction and then loading is applied in both the X any Y directions. (ii) prestretching the specimen in the Y direction and loading is applied in the X direction. (iii) prestretching the specimen in the Y direction and loading is applied in the Y direction.

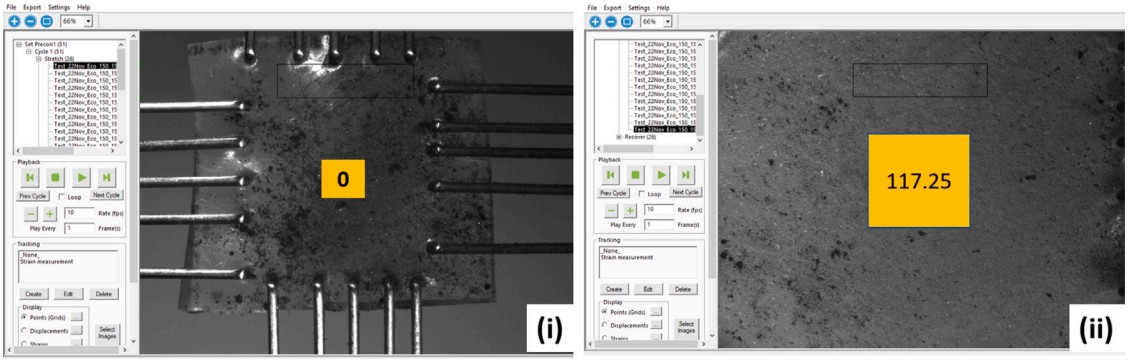

Fig. 6. DIC technique utilized in Biaxial Testing Machine to obtain strain maps.

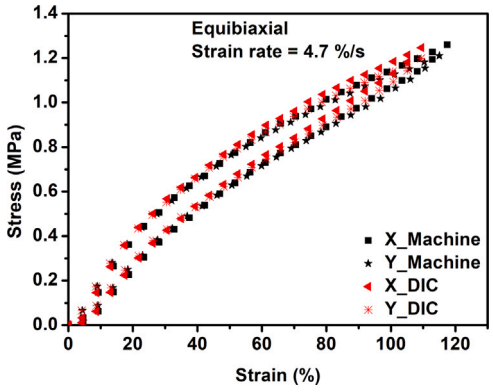

Fig. 7. Stress–strain graphs showing the comparison between DIC and machine data for equibiaxial loading at a strain rate of 4.7%/s.

file menu as shown in Fig. 6. Then, an appropriate test file is selected that contains all the information related to the test. After selecting the test file, the software can display images and data. To measure the strain through DIC, a square is created on the first specimen as shown in Fig. 6(i) by clicking create button and selecting the grid option. The source and target images are preset through the create button before tracking all points. After tracking all the points, the strains for all images can be visualized by just selecting them. For example, the final image is selected to obtain the strain map of 117.25 for the X direction as shown in Fig. 6 (ii). Similarly, the strain in the Y direction can be obtained by selecting the ϵ_y option from the strain menu as shown in the lower left of Fig. 6. For representation, all the strain maps obtained for different strain rate conditions under biaxial loading are shown in Fig. 4. Before each experiment, graphite powder is sprinkled over the specimen to get better tracking of particles for strain measurement through DIC. Moreover, to examine the effect of boundary conditions, we have compared the stress–strain graphs from the data obtained by the machine and from the calculation through image analysis as shown in Fig. 7 at a particular condition of equibiaxial loading. For a uniform

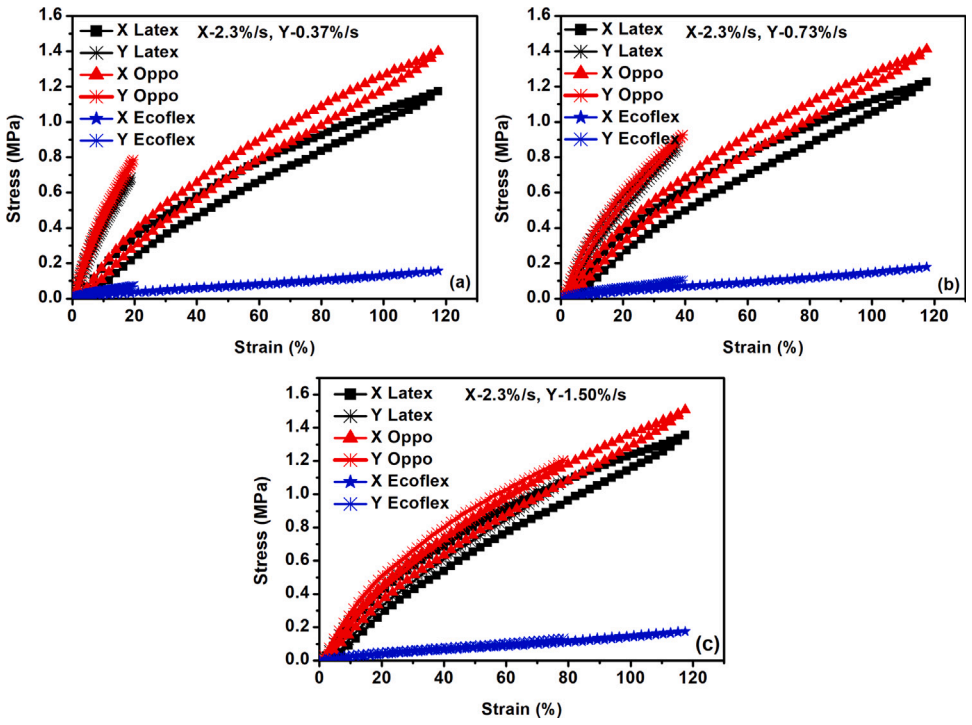

Fig. 8. Biaxial loading–unloading curves showing hysteresis losses (%) for Latex, Oppo and Ecoflex at different strain rates in the Y direction for (a) X-2.3%/s, Y-0.37%/s (b) X-2.3%/s, Y-0.73%/s (c) X-2.3%/s, Y-1.50%/s.

Table 1
Biaxial hysteresis losses (%) variations for Latex, Oppo and Ecoflex under different strain rates in the Y direction.

Materials/Strain Rates (Y)	X-2.3%/s, Y-0.37%/s	X-2.3%/s, Y-0.73%/s	X-2.3%/s, Y-1.5%/s
Latex	10.60 ± 0.04, 0.916 ± 0.04	11.07 ± 0.04, 2.34 ± 0.03	13.32 ± 0.02, 7.31+0.03
Oppo	10.18 ± 0.03, 2.54 ± 0.03	10.53 ± 0.02, 1.86 ± 0.02	11.24 ± 0.04, 1.02 ± 0.04
Ecoflex	0.50 ± 0.02, 0.07 ± 0.02	0.65 ± 0.03, 0.17 ± 0.04	0.89 ± 0.02, 0.41 ± 0.01

stretching, the maximum stretch is fixed up to a maximum of 117% for different strain rates. Stretching more than this value will bring nonuniformity in the strain measurement because tearing may start from the gripping region. The machine provides displacement taking into account the distance between grip to grip. As it can be seen that the graphs obtained from both methods are in quite good agreement. Therefore, slight misalignments in gripping regions due to the tines play a negligible effect on the presented results up to smaller stretches. Hence, in the current contribution, we have presented all the results from the data obtained by the machine.

3. Results and discussions

3.1. Effect of different polymers on loading–unloading curves ($X\,strainrate = 2 \times Y\,strainrate$) at three different strain rates

Fig. 8 shows the biaxial loading–unloading curves for all three materials. In this set of experiment, the strain rate in the direction of the X-axis is fixed at 2.3%/s while the strain rates in the Y direction varies as 0.37%/s, 0.73%/s and 1.50%/s, respectively for each material. The hysteresis losses are obtained for each case and included in Table 1 with standard deviations [47].

The hysteresis losses, presented in Table 1, are calculated from the following equation [31,38]:

$$\text{Hysteresis Loss}(\%) = \frac{\left|\text{Area (Loading Curve)}\right| - \left|\text{Area (Unloading Curve)}\right|}{\left|\text{Area (Loading Curve)}\right|} \times 100 \quad (1)$$

It is shown in Table 1, that the hysteresis losses (%) for Latex increase in both X and Y directions with increasing strain rates only in the Y direction. The hysteresis corresponds to the amount of energy loss in a loading–unloading cycle of polymeric materials and is related to the inelastic dissipation mechanism arising due to viscoelasticity [50]. The same increasing pattern is obtained for Oppo and Ecoflex. This is because, at higher strain rates, the viscoelastic materials produce more frictional losses due to the fast sliding of chains and entanglements over each other [31,38]. It is also shown that silicone-based Ecoflex polymer is producing the least hysteresis losses (%) but the highest hysteresis losses (%) is obtained for Latex at a particular strain rate condition. The hysteresis loss in Ecoflex is observed to be the least because it might contain the least number of chains and entanglements as compared to the other two materials, see similar behavior in [51–54]. On the other hand, Latex experiences the highest hysteresis losses because it might contain more crosslinks and entanglements. This induces the highest frictional losses due to the sliding of chains and entanglements over each other. Hence, the experimental results show that the least and highest hysteresis losses (%) are observed in Ecoflex and Latex, respectively at a particular condition.

Secant elastic modulus (Stiffness) is also calculated and included in Table 2. The stress is divided with the strain value at 20% to get the secant elastic modulus of the material. It is observed that stiffness is also increasing with strain rates. This phenomenon is caused because at higher strain rates, the chains and entanglements in the material have very little time for stress relaxation at higher strain rates [55]. Also, the stiffness observed in Ecoflex is very less as compared to the other materials like Latex and Oppo at a particular strain rate condition. This shows that Ecoflex is less viscous than Oppo and Latex.

Table 2
Biaxial stiffness (kPa) (at 20% strain) variations for Latex, Oppo and Ecoflex under different strain rates in the Y direction.

Materials/Strain Rates (Y)	X-2.3%/s, Y-0.37%/s	X-2.3%/s, Y-0.73%/s	X-2.3%/s, Y-1.5%/s
Latex	1777.21 ± 2.45, 3661.21 ± 3.05	1933.33 ± 3.26, 2944.44 ± 4.52	2166.66 ± 3.25, 2245.98 ± 4.5
Oppo	2000.05 ± 4.01, 4188.88 ± 3.25	2032.08 ± 3.26, 3111.11 ± 3.85	2333.33 ± 4.25, 2666.66 ± 3.85
Ecoflex	211.11 ± 3.36, 364.83 ± 2.25	224.59 ± 4.56, 333.58 ± 3.50	227.77 ± 2.45, 261.11 ± 2.65

Table 3
Biaxial hysteresis losses (%) (X-Stretch = 2 x Y-Stretch) for Latex, Oppo and Ecoflex under different strain rates.

Materials/Strain rates	X-1.1%/s, Y-0.5%/s	X-4.7%/s, Y-2.3%/s	X-11.7%/s, Y-5.7%/s
Latex	11.50 ± 0.04, 4.14 ± 0.04	12.99 ± 0.03, 4.54 ± 0.05	14.68 ± 0.04, 4.62 ± 0.04
Oppo	6.01 ± 0.02, 2.04 ± 0.05	8.91 ± 0.03, 2.73 ± 0.03	9.01 ± 0.05, 3.09 ± 0.05
Ecoflex	0.60 ± 0.05, 0.20 ± 0.03	0.74 ± 0.05, 0.23 ± 0.04	1.11 ± 0.02, 0.25 ± 0.03

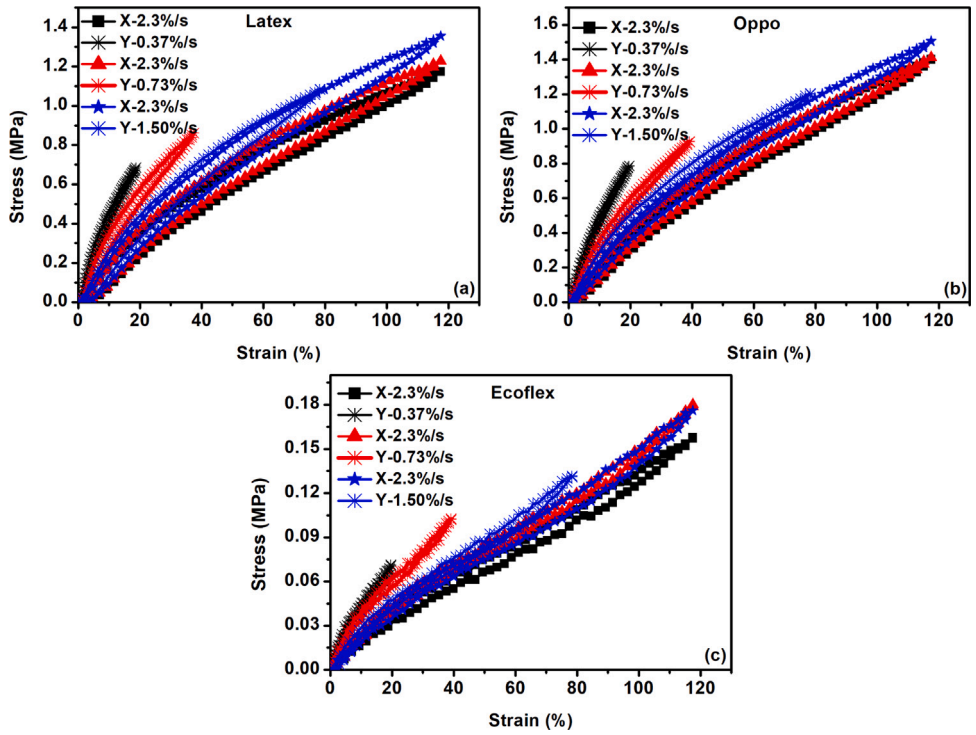

Fig. 9. Biaxial loading–unloading curves showing hysteresis losses (%) for three strain rates at different strain rates in the Y direction for (a) Latex (b) Oppo and (c) Ecoflex.

3.2. Effect of strain rates on loading–unloading curves ($X strainrate = 2 \times Y strainrate$) for three different materials

Fig. 9 represents loading–unloading curves at three different strain rates for the three different polymers. In each strain rate condition, the strain rate in the X-direction is kept constant at 2.3%/s but the strain rates in the Y direction are changed as 0.37%/s, 0.72%/s, and 1.50%/s, respectively. With the increasing strain rates, it is observed that the stiffness is highest when the biaxial deformation takes place at a slower strain rate in the Y-direction. This is because, at a particular strain rate, more force/stress is observed along the axis of the slower strain rate (Y-axis) as shown in Fig. 9(a), (b), and (c) for all the materials, respectively. However, from Table 2, the stiffness along the X-axis is observed to be least for a strain rate of (X-2.3%/s, Y-0.37%/s) and highest for (X-2.3%/s, Y-1.5%/s) for a particular material. The reason is already discussed in Section 3.1. Due to a slower strain rate in the Y direction, the chains of the polymer are more stretched in the X direction, therefore needing more force from the Y direction to achieve a particular strain as shown in Fig. 9. This makes the material stiffer in the Y direction. The strain rate in the Y direction is chosen as 5.7%/s [33] and make it double for the X-axis as 11.7%/s as shown in Fig. 12(a). Then, the strain rate in the X and Y directions are divided by half as shown in Fig. 12(a) and (b), respectively to understand the biaxial strain rate effect for all the polymers.

3.3. Biaxial loading–unloading curves at different strain rates in the X and Y directions for the three materials

Fig. 10 shows the loading–unloading curves varying the strain rates in both X and Y directions. In each particular condition, the strain rate in the X direction is kept twice that in the Y direction as shown in Fig. 10(a), (b), and (c). Hysteresis losses (%) obtained in each case are shown in Table 3. It is observed that with the increase in strain rates, the hysteresis losses (%) increase in both X and Y directions. However, the hysteresis losses (%) are investigated to be least for Ecoflex and highest for Latex material. The reason for an increase in the hysteresis losses (%) with the strain rates is already discussed in the earlier section.

The stiffness in both the X and Y directions increases with strain rates as shown in Table 4. For example, stiffness for Latex at a strain rate of (X = 1.1%/s, Y = 0.5%/s) is found to be 1780.15 kPa and 2200.01 kPa, respectively. The stiffness increases up to 1966.52 kPa and 2454.54 kPa at a higher strain rate of (X = 11.75%/s, Y = 5.75%/s). It is observed that the stiffness in the Y direction is always more as compared to that in the X direction at a particular strain rate condition.

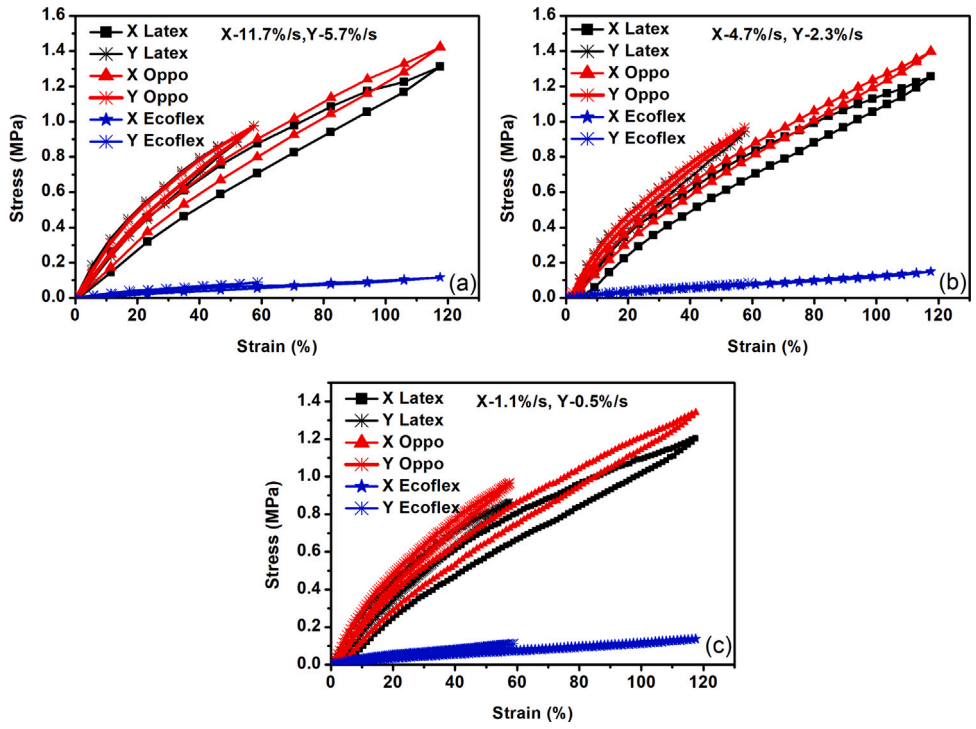

Fig. 10. Biaxial loading–unloading curves for Latex, Oppo and Ecoflex at different strain rates of (a) X-11.75%/s, Y-5.75%/s (b) X-4.7%/s, Y-2.3 %/s and (c) X-1.1%/s, Y-0.5%/s.

Table 4
Biaxial stiffnesses (kPa) (at 20% strain) for Latex, Oppo and Ecoflex under different strain rates (X-Stretch = 2 x Y-Stretch).

Materials/Strain Rates	X-1.1%/s, Y-0.5%/s	X-4.7%/s, Y-2.3%/s	X-11.7%/s, Y-5.7%/s
Latex	1780.15 ± 3.54, 2200.01 ± 3.81	1817.39 ± 4.01, 2227.07 ± 3.93	1956.52 ± 4.21, 2454.54 ± 3.85
Oppo	1826.08 ± 3.57, 2304.04 ± 4.02	1869.56 ± 2.89, 2318.18 ± 3.01	1982.60 ± 3.81, 2409.09 ± 3.43
Ecoflex	171.42 ± 3.24, 257.14 ± 4.02	153.91 ± 4.21, 191.30 ± 4.32	147.82 ± 3.52, 185.65 ± 4.02

Table 5
Equibiaxial hysteresis losses (%) for Latex, Oppo and Ecoflex under different strain rates.

Materials/Strain Rates	X, Y-4.7%/s	X, Y-1.1%/s	X, Y-0.78%/s
Latex	12.24 ± 0.05, 12.01 ± 0.05	11.89 ± 0.06, 11.82 ± 0.06	11.01 ± 0.03, 10.98 ± 0.02
Oppo	11.03 ± 0.03, 11.02 ± 0.03	10.85 ± 0.05, 10.82 ± 0.05	10.50 ± 0.02, 10.48 ± 0.02
Ecoflex	1.25 ± 0.04, 1.24 ± 0.04	1.20 ± 0.05, 1.21 ± 0.04	1.15 ± 0.04, 1.16 ± 0.03

The reason for this is that a higher strain rate in the X direction causes the chains to stretch faster and hence more force is required from the Y direction at a particular strain [36]. This keeps the stiffness in the Y direction to be appreciably higher as compared to the transverse X direction.

3.4. Effect of strain rates on loading–unloading curves for three different materials

From Fig. 11, the effect of biaxial loading–unloading curves keeping the Y-directional strain rate half to the X-directional strain rate (X-11.7%/s, Y-5.7%/s) and then decreasing the strain rates to (X-4.7%/s, Y-2.3%/s) and (X-1.1%/s, Y-0.5%/s), respectively as shown in Fig. 11(a), (b) and (c) for Latex, Oppo and Ecoflex, respectively. It is observed that stress at a particular strain in both the X and Y directions decreases with strain rates. This shows the strain rate dependency of the polymeric materials under biaxial loading. The reasons are also discussed in Section 3.1 in detail. The stiffnesses in the X and Y directions are detailed in Table 4. The stiffnesses increase with strain rates but their values are always more in the Y direction as shown in each case. Also, the values of stiffness for Ecoflex are almost 10 times lesser than that of Latex and Oppo.

3.5. Equibiaxial loading–unloading curves at different strain rates for three materials

Equibiaxial loading–unloading curves for three different materials at three different strain rates are shown in Fig. 12. The strain rates selected for different equibiaxial loading are 0.78%/s, 1.1%/s, and 4.7%/s respectively. The highest strain rate is selected to be 4.7%/s, similar to Katlseis et al. [33] and then decreasing to 1.1%/s and 0.78%/s for stretching the specimen for 100s and 150s, respectively. It is observed that with increasing strain rates, hysteresis losses (%) increase This increase in hysteresis losses with increasing strain rates is valid for all three materials as shown in Table 5. However, for Ecoflex material, the hysteresis loss is least as compared to the other two materials. Also, stiffnesses are shown in Table 6 for different strain rates. Stiffness is highest for higher strain rates and vice versa for all the materials. But, the stiffness of Oppo under equibiaxial loading is very high as compared to Ecoflex at a particular strain rate. Stiffness is highest in Oppo and lowest in Ecoflex material. This may be because the chains and entanglements in Oppo are densely cross-linked. Therefore, stress acting at a particular strain is observed to be more for Oppo leading to the highest stiffness as shown clearly in Fig. 12(a), (b), and (c). It is also shown in Table 6 that stiffness is almost the same in both X and Y directions under equibiaxial loading. This

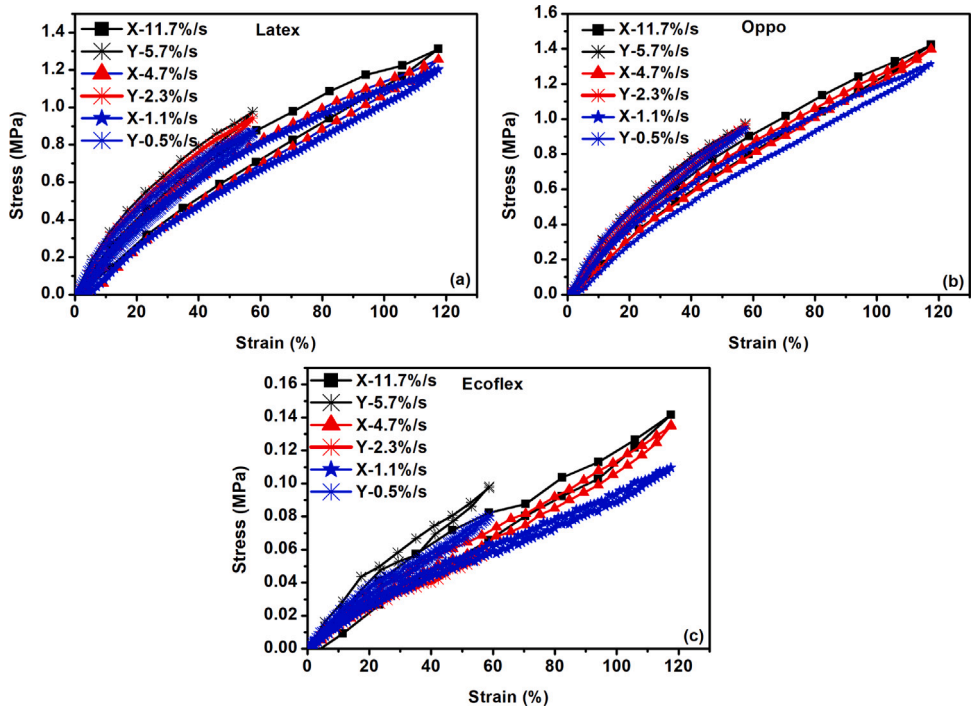

Fig. 11. Biaxial loading–unloading curves showing hysteresis losses (%) for three strain rates at different strain rates in both direction for (a) Latex (b) Oppo and (c) Ecoflex.

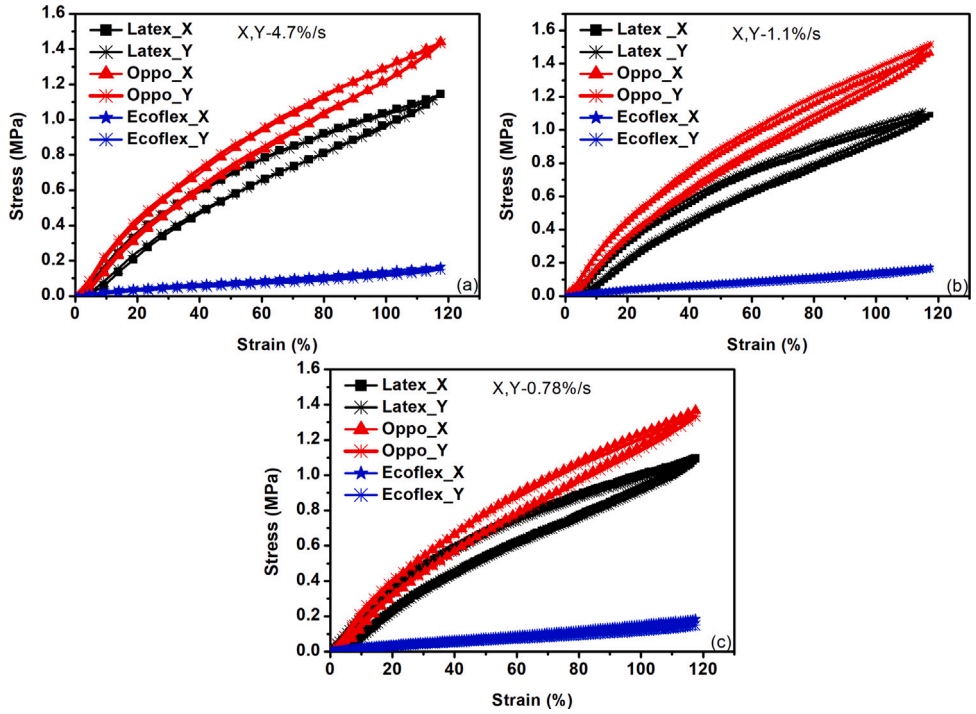

Fig. 12. Equibiaxial loading–unloading curves for latex, Oppo and Ecoflex at different strain rates of (a) 4.7%/s (b) 1.1%/s and (c) 0.78%/s.

Table 6
Equibiaxial stiffnesses (kPa) (at 20% strain) for Latex, Oppo and Ecoflex under different strain rates.

Materials/Strain Rates	X, Y-4.7%/s	X, Y-1.1%/s	X, Y-0.78%/s
Latex	1827.77 ± 2.56, 1830.55 ± 3.26	1777.77 ± 3.56, 1710.91 ± 4.25	1604.25 ± 3.25, 1610.52 ± 4.35
Oppo	2166.66 ± 3.28, 2170.12 ± 4.26	2010.15 ± 3.56, 2009.23 ± 4.23	2000.92 ± 4.26, 190.19 ± 3.51
Ecoflex	227.22 ± 2.35, 226.12 ± 3.25	220.15 ± 3.25, 222.15 ± 4.35	205.10 ± 4.26, 206.35 ± 5.25

is because, during equibiaxial loading, the chains and entanglements deform homogeneously due to equal application of forces from both directions, simultaneously [36,37].

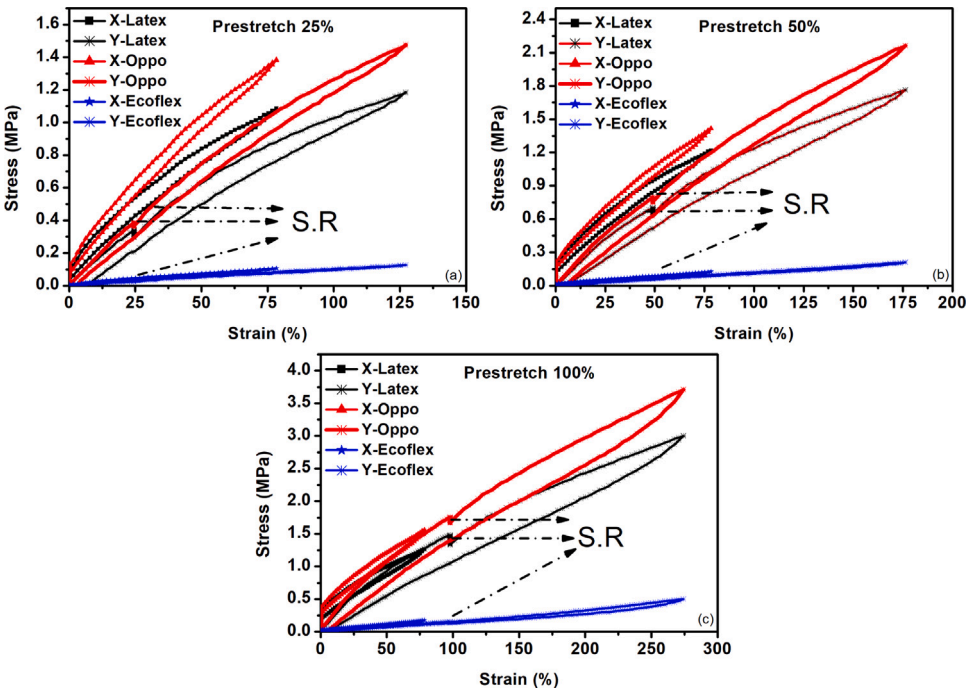

Fig. 13. Biaxial loading–unloading curves at different prestretch values of (a) 25%, (b) 50% and (c) 100% for Latex, Oppo and Ecoflex.

Table 7
Stiffness (at 10% strain after prestretch) variations under different prestretch (Y dir) and loading in the Y direction up to different maximum strains.

Materials/Prestretch	Prestretch = 25%X, Y	Prestretch = 50%X, Y	Prestretch = 100%X, Y
Latex	2320.09 ± 2.18, 1424.56 ± 1.54	2803.92 ± 1.18, 1765.12 ± 2.35	3296.65 ± 3.87, 1809.12 ± 4.88
Oppo	2816.51 ± 3.25, 1658.71 ± 3.14	3065.34 ± 3.24, 2009.52 ± 2.24	3826.81 ± 3.15, 2673.35 ± 4.56
Ecoflex	300.59 ± 4.26, 212.31 ± 3.25	401.65 ± 3.15, 250.51 ± 3.67	700.12 ± 2.56, 277.77 ± 3.25

3.6. Biaxial loading–unloading curves (X and Y directions) for different prestretch in the Y directions for different materials

The effect of different Y-directional prestretch and loading–unloading curves in the X and Y directions are shown in Fig. 13. The effect of different prestretch values as 25%, 50%, and 100% for Latex, Oppo, and Ecoflex are shown in Fig. 15(a), (b), and (c), respectively. To this end, the specimen is first stretched in the Y direction up to the required prestretch ratio and then left for stress relaxation (S.R) for a period of 480s. The stress relaxation (%) after prestretch can be calculated as follows [38,47]:

$$\text{StressRelaxation (\%)} = \frac{\left|\begin{matrix}\text{MaxStress}\\(\text{AfterLoading})\end{matrix}\right| - \left|\begin{matrix}\text{Stress}\\(\text{AfterRelaxation})\end{matrix}\right|}{\left|\begin{matrix}\text{MaxStress}\\(\text{AfterLoading})\end{matrix}\right|} \times 100 \quad (2)$$

Then, loading–unloading in both the X and Y directions takes place. The stiffnesses are calculated for each case and included in Table 7. It is clearly shown from Table 7 that at a particular prestretch ratio, the stiffnesses in both the X and Y directions are maximum for Oppo but minimum for Ecoflex. This is because stress acting at a particular strain in the Y direction is always higher as shown in Fig. 13. Therefore, the stiffness is always higher in the Y direction, valid for all the materials. Also, it is observed that stiffnesses are highest in Oppo and least in Ecoflex (approx. 10 times lesser). This is because Ecoflex is a comparatively softer material due to a smaller number of chains and entanglements as compared to that of Oppo [33,52]. Therefore, stress at a particular strain in Oppo is always highest among all the materials and lowest in Ecoflex. Hence, it is also observed in Table 7 that the stiffness of Ecoflex is very less as compared to the Oppo at a particular prestretch ratio. The hysteresis losses (%) are also calculated and shown in Table 8. It is clearly shown that the hysteresis losses (%) are always highest for Latex and least for Ecoflex at a particular prestretch ratio. Moreover, with the increase in prestretch, the hysteresis losses (%) increase appreciably in the prestretched direction as compared to that in the lateral (X) direction. The hysteresis losses in the X direction are smaller than those in the Y direction. This is because the chains in the Y-direction first uncoil and then the stretching of the chain starts which enables the material to stretch more in the Y direction than that in the X-direction. This smaller stretching in the X direction induces less frictional losses in this direction resulting in smaller hysteresis losses (%) for all three materials.

3.7. Biaxial loading–unloading curves (X directions) for different prestretch in the Y directions

From Fig. 14, loading–unloading curves are plotted for Latex, Oppo, and Ecoflex materials under different prestretch values ranging from 50% to 200% as discussed in Case 5. In this case, the material is first prestretched in the Y direction and then the load is applied from the X direction to complete a cycle at a strain rate of 2%/s. The hysteresis losses in a cycle are then obtained and shown in Table 9. It is observed that as the prestretch increases, the hysteresis losses (%) also increase. This increase in hysteresis loss is due to an increase in the stretching of the chains and entanglements in the Y direction due to higher prestretch values. This is because as the polymers are stretched in the Y direction, their width increases causing more frictional losses in the material [25]. Variation of stiffness is also shown in the same table, Table 9. Herein, it is also shown that the stiffness decreases with increasing prestretch. This decrease in the stiffness is due to the reason

Table 8
Biaxial (X and Y) hysteresis losses for Latex, Oppo and Ecoflex under different prestretch (Y dir.)

Materials/Prestretch	Prestretch 25%X, Y	Prestretch 50%X, Y	Prestretch 75%X, Y
Latex	6.81 ± 0.02, 13.91 ± 0.03	7.50 ± 0.04, 28.18 ± 0.05	10.09 ± 0.03, 94.16 ± 0.04
Oppo	6.01 ± 0.03, 12.98 ± 0.04	6.18 ± 0.04, 10.64 ± 0.02	9.10 ± 0.05, 90.45 ± 0.04
Ecoflex	2.21 ± 0.03, 6.18 ± 0.04	0.59 ± 0.02, 1.80 ± 0.02	0.41 ± 0.04, 0.64 ± 0.03

Table 9
Hysteresis losses (%) and stiffnesses (%) under different prestretch (Y dir) and loading in X-direction.

Materials/Prestretch	Y-Prestretch = 50% Hysteresis Loss (%), Stiffness (MPa)	Y-Prestretch = 100% Hysteresis Loass (%), Stiffness (MPa)	Y-Prestretch = 200% Hysteresis Loss (%), Stiffness (MPa)
Latex	10.94 ± 0.02, 1555.55 ± 2.45	12.37 ± 0.03, 1433.33 ± 2.54	16.09 ± 0.01, 1288.88 ± 2.35
Oppo	14.24 ± 0.03, 2777.77 ± 3.25	18.23 ± 0.04, 2500.00 ± 2.35	30.24 ± 0.02, 2401.33 ± 3.25
Ecoflex	0.90 ± 0.01, 161.11 ± 4.51	1.07 ± 0.02, 140.33 ± 3.56	2.54 ± 0.01, 133.88 ± 4.01

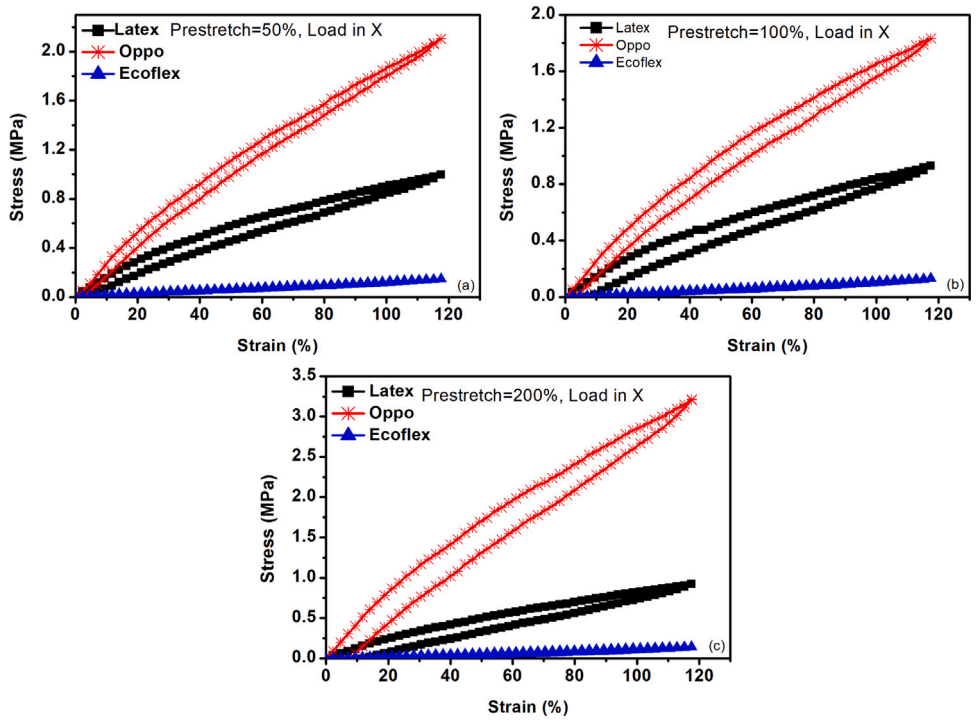

Fig. 14. Loading–unloading curves for Latex, Oppo and Ecoflex at different prestretch values of (a) 25%, (b) 50% and (c) 100% in the Y direction and loading in the X direction.

that if the material is stretched in one direction and load is applied from the transverse direction, the initial forces acting on chains of the material are always lower as shown in Fig. 16 [35].

3.8. Biaxial loading–unloading curves (Y directions) for different prestretch in the Y directions and fixed maximum stretch

In Fig. 15, loading–unloading curves are plotted under different prestretch values of 25%, 50%, and 75% in the Y direction for Latex, Oppo, and Ecoflex. All the tests are conducted up to a maximum strain of 130% at a fixed strain rate of 2%/s. The specimen is first prestretched and left for stress relaxation for about 480s [47] and then loading–unloading is applied to reach the initial specimen size mimicking the span morphing. The hysteresis losses (%) are observed to be increasing with prestretch for all three materials. However, the hysteresis loss is maximum for Latex and lowest for Ecoflex at a particular prestretch value and strain rate. The reasons are already detailed in the earlier sections. This increase in hysteresis losses (%) with the increase in prestretch in the Y direction is because with stretching, strain hardening increases. After applying force in the same Y direction, the strain hardened chains are difficult to stretch further. This induces more forces during stretching and hence the material becomes stiffer in the Y direction and it creates more hysteresis losses (%) in that direction. The hysteresis losses (%) and stiffnesses (kPa) are also calculated for each material and elaborated in Table 10. The stiffnesses are calculated in this case at 10% strain after each prestretch ratio. The stiffness is calculated at 10% prestretch because the stress–strain graph is linear in this region after prestretch. It is shown in Table 11 that the stiffness decreases with the prestretch values. The stiffnesses are decreasing because the slopes are decreasing with the strain for all the materials as shown in Fig. 16. Also, the stiffness is observed to be highest in Oppo and lowest in Ecoflex at a particular prestretch and strain rate condition. The force value, observed for the soft Ecoflex, is very small and therefore, the machine produces a slight variation in the data as shown in Fig. 16(c). The stress relaxation (%) after each prestretch is also shown in Table 10. It is observed that the stress relaxation (%) decreases with the increasing prestretch. This decrease is because at higher prestretch the chains are more elongated and there is very little stress relaxation at this point due to elongated chains [56]. On the other hand, for smaller prestretch value, the chains are little stretched and therefore, they easily uncoil to achieve more relaxation of stress.

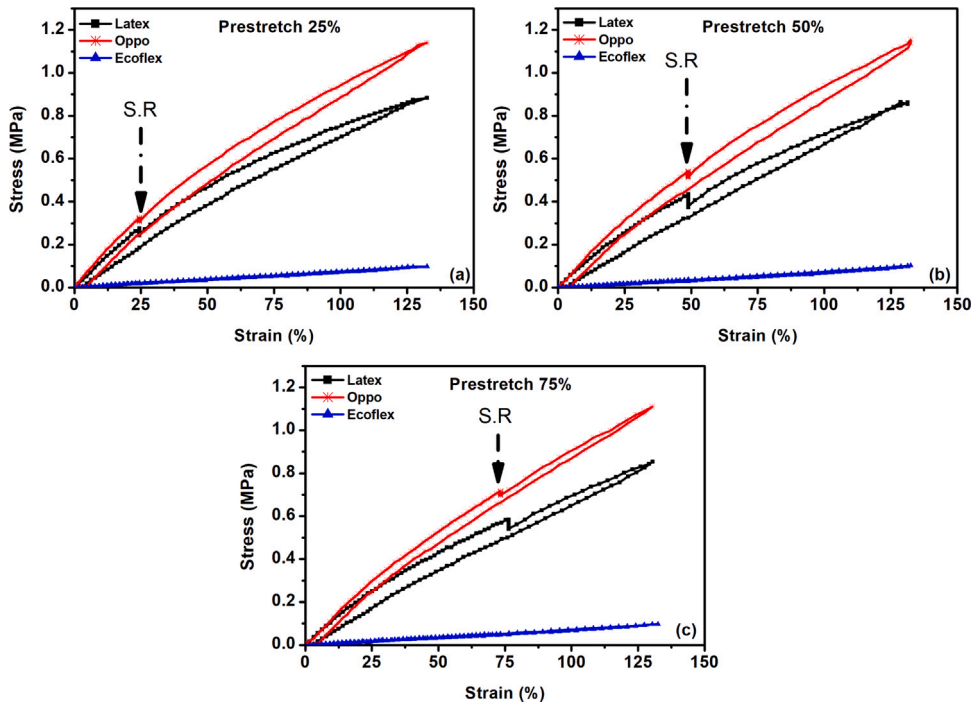

Fig. 15. Loading–unloading curves for Latex, Oppo and Ecoflex at different prestretch values of (a) 25%, (b) 50% and (c) 75% in the Y direction and loading in the Y direction up to a fixed maximum strain of 130%.

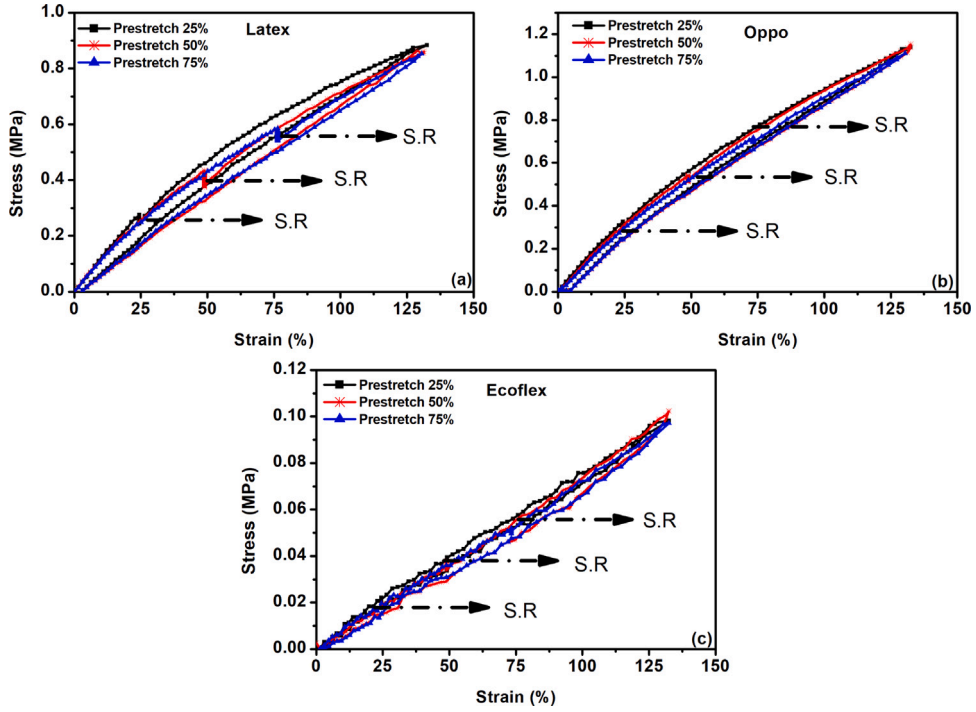

Fig. 16. Loading–unloading curves for different prestretch values of 25%, 50% and 75% at different materials (a) Latex (b) Oppo and (c) Ecoflex in the Y direction and loading in the Y direction up to a fixed maximum strain of 130%.

Table 10
Hysteresis losses (%) and stress relaxations (%) under different prestretch values (Y dir) and loading in the Y direction for a maximum fixed strain up to 130%.

Materials/Prestretch	Prestretch = 25% Hysteresis losses (%), Stress relaxation (%)	Prestretch = 50% Hysteresis losses (%), Stress relaxation (%)	Prestretch = 75% Hysteresis losses (%), Stress relaxation (%)
Latex	7.57 ± 0.03, 10.83 ± 0.02	7.87 ± 0.02, 8.23 ± 0.01	7.96 ± 0.01, 7.22 ± 0.02
Oppo	5.14 ± 0.01, 6.13 ± 0.01	6.51 ± 0.03, 5.16 ± 0.02	6.97 ± 0.02, 2.78 ± 0.03
Ecoflex	0.47 ± 0.01, 1.5 ± 0.03	0.52 ± 0.03, 1.2 ± 0.03	0.63 ± 0.02, 1 ± 0.02

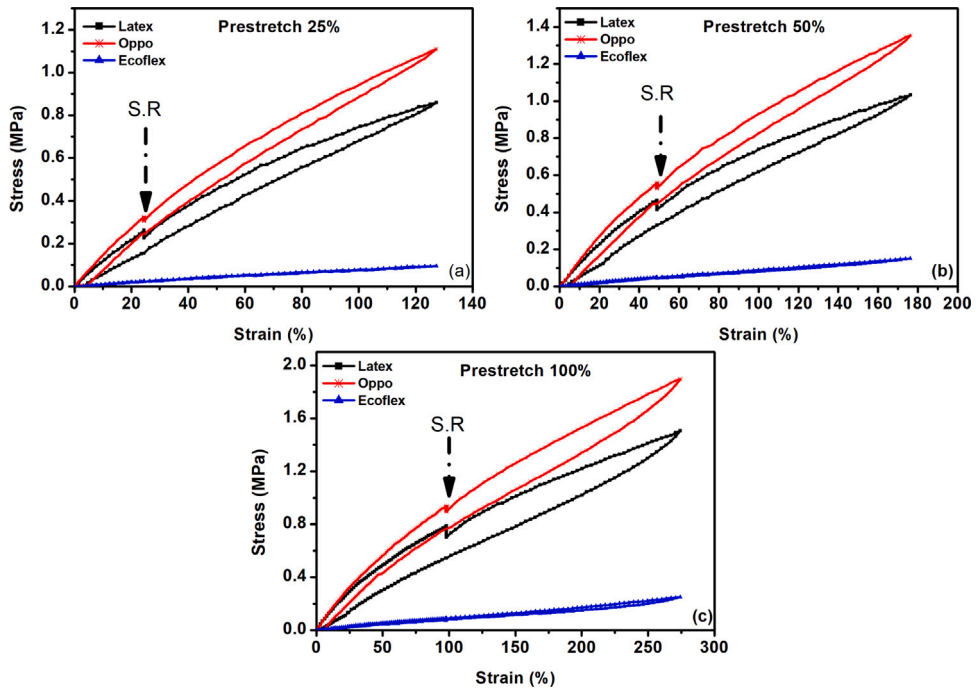

Fig. 17. Loading–unloading curves for Latex, Oppo and Ecoflex at different prestretch values of (a) 25%, (b) 50% and (c) 100% in the Y direction and loading in the Y direction up to a different maximum strains of 130%, 180% and 270%, respectively.

Table 11
Representation of stiffness under different prestretch values (Y dir) and loading in the Y direction.

Materials/Prestretch	Prestretch = 25%	Prestretch = 50%	Prestretch = 75%
Latex	1020.17 ± 2.18	797.74 ± 3.67	714.95 ± 2.56
Oppo	1233.42 ± 3.15	1058.26 ± 2.45	942.04 ± 3.46
Ecoflex	83.57 ± 4.58	70.96 ± 4.27	60.19 ± 4.37

Table 12
Representation of hysteresis losses (%) under different prestretch (Y dir) and loading in the Y direction up to different maximum strains.

Materials/Prestretch	Prestretch = 25%	Prestretch = 50%	Prestretch = 100%
Latex	9.40 ± 0.02	16.77 ± 0.04	48.49 ± 0.02
Oppo	8.37 ± 0.04	15.58 ± 0.03	41.71 ± 0.02
Ecoflex	0.33 ± 0.06	1.08 ± 0.07	3.77 ± 0.06

3.9. Biaxial loading–unloading curves (Y directions) for different prestretch in the Y directions and different maximum strains

Fig. 17 shows the loading–unloading plots for different Y direction prestretch values of 25%, 50%, and 100% wherein, after prestretch, the maximum Y directional strains of the specimen are 130%, 180% and 275%, respectively at a fixed load–unload strain rate of 2%/s. The comparison of hysteresis losses from the loading–unloading graphs for different materials and prestretch values obtained are shown in Table 12. From Table 12, the hysteresis losses (%) at a fixed prestretch ratio are highest for Latex and least for Ecoflex. The reasons are well explained in the earlier sections. However, with the increase in the prestretch values, the hysteresis losses increase appreciably because the maximum strain is also increasing as shown in Fig. 17(a), (b), and (c), respectively. Due to increasing maximum strains, more stretching takes place that induces higher frictional losses due to slippage of chains and entanglements over each other [48,51,52].

4. Discussion on the scientific insights of the morphing wing under various conditions

All the results obtained under different biaxial strain rates and various prestretched conditions have important scientific contributions in the broad field of morphing wings undergoing multiaxial deformation. Moreover, to understand the relevance of biaxial results on Latex, Oppo, and Ecoflex, the following subsections are included:

4.1. Different polymeric materials applied in the morphing wing

In polymorphing wing (for example capable of span and camber morphing), the implementation of new lightweight polymeric materials meeting the requirement of low in-plane and high-out of plane stiffness is required [16,38]. To this end, silicone polymers are used in the polymorphing wing [2,18–20]. Also, natural-rubber-based polymers, Latex is applied in the polymorphing wing [13,14]. A good polymer for polymorphing skin must have minimum stiffness and the least hysteresis losses (%) to minimize the actuation force required to morph in the biaxial directions. From the comparative results between natural rubber polymers (Latex and Oppo) and silicone polymers (Ecoflex), the stiffness and hysteresis losses (%) are least for Ecoflex and highest for Latex as shown in Tables 1–4. Therefore, silicone-based Ecoflex is best suited for the polymorphing application. The representative examples of Silicone and Latex polymer utilized in the morphing wing are shown in Fig. 18(a) and (b), respectively.

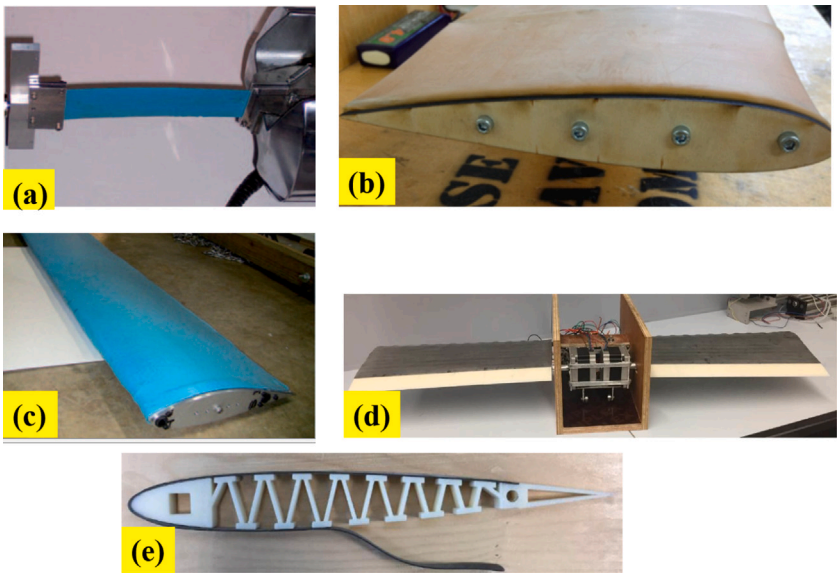

Fig. 18. Representation of different polymers used in morphing wing as (a) Silicone polymer [2] (b) Latex polymer [24] (c) span morphing (monomorphing) [57] (d) chord and camber (polymorphing) [13] (e) prestretched polymer in the morphing wing [13].

4.2. Different biaxial strain rates in the morphing wing

In the context of polymorphing wings, morphing the different degrees of freedom can result in biaxial loading of the skin at different strain rates. For example, consider a polymorphing wing capable of span extension and camber variation. Span extension occurs at a much slower rate when compared to camber variations. This is because camber variations are usually used for flight control which is usually quite fast. On the other hand, span extension is usually used to enhance flight performance, and therefore the actuation rate is usually low [9, 24]. At higher strain rates the hysteresis losses (%) and stiffness are more in the biaxial modes. For example, Fig. 10 represents a typical example of different strain rates in the X and Y direction resembling span and camber morphing, respectively for Latex, Oppo, and Ecoflex. The stiffness in the direction of a slower strain rate is always higher. Comparing all the three materials, stiffness is observed least in Ecoflex as shown in Table 2. Fig. 18(c) represents the span morphing wing deformation in the X direction while Fig. 18(d) mimics the chord and camber morphing deforming in both the X and Y directions.

4.3. Application of polymeric skin with different prestretch values

Generally, the polymeric skin is prestretched to reduce wrinkle formation and to increase the out-of-plane load-bearing capacity of the skin [2,13]. For example, for span morphing, the skin is first prestretched in the Y direction, and then loading is applied in the same Y direction [24]. The stiffness increases with prestretch values, therefore higher actuation force is required with a higher prestretched skin as shown in Table 9. Moreover, in the example of the polymorphing wing capable of camber and span morphing, the skin is deformed in both directions (X and Y), respectively [13]. As shown in Tables 7 and 8, the stiffness during camber morphing (X) is more as compared to the stiffness in the span morphing (Y). However, stiffness is always less for the Ecoflex and highest for the Oppo under different prestretch conditions. The prestretched Latex skin utilized in the morphing wing is shown in Fig. 18(e).

4.4. Actuation force requirement in the morphing wing under various conditions

The material for minimum actuation force requirement is an important aspect of designing morphing wings [14,28]. The stiffness of prestretched Ecoflex is found to be very small (10 times lesser than Oppo) as shown in Fig. 17. Hence, silicone-based Ecoflex material is the best candidate material for span morphing exhibiting less stiffness at higher strains. The current investigations also reveal that the prestretch in the Y direction and loading in the X direction resembles camber morphing as shown in Fig. 14. It can be concluded that Latex is a better material than Oppo to be used in the camber morphing as the stiffness of Latex is less than the Oppo at a particular strain rate. Hence less actuation force is required for Latex than Oppo.

5. Conclusion

This paper presented a comprehensive mechanical characterization of Latex, Oppo, and Ecoflex deforming in the biaxial mode. The effect of strain rates and prestretch ratios on the skin stiffness and hysteresis losses were assessed and compared. The stiffness and hysteresis losses were least in Ecoflex and highest in Latex at a fixed strain rate. Hysteresis losses (%) and stiffness increased with the prestretch ratio when loading was applied in the prestretch direction such as in the cases with span morphing wings. For morphing wing applications, the skin is usually prestretched and then implemented on the wing structure. Experimental results revealed that when the skin deforms at a fixed strain rate in the Y direction (similar to monomorphing wings), hysteresis losses (%) increased but stiffness decreased for all the materials. When the skin deformed in both directions (X and Y) (similar to a polymorphing wing capable of span and camber morphing) hysteresis losses (%) and stiffness in the X and Y direction increased with the strain rates but both values were more in the Y direction at a particular strain rate. Furthermore, results showed that the skin deforming biaxially was stiffer in the direction of slower actuation speed. However, the stiffnesses become equal at equal actuation speeds in both directions (X and Y). Also, the experimental investigations showed biaxial strain rate dependency in all the polymers studied. Finally, the major conclusion drawn from the comparative results was that silicone-based Ecoflex polymer is the best candidate material for morphing applications (monomorphing and polymorphing). This is because it was associated with the smallest stiffness that required a relatively small actuation force.

CRediT authorship contribution statement

Dilshad Ahmad: Conception and design of study, Acquisition of data, Analysis and/or interpretation of data, Writing – original draft, Writing – review & editing. **Rafic M. Ajaj:** Analysis and/or interpretation of data, Writing – review & editing. **Mohammadreza Amoozgar:** Writing – review & editing.

Declaration of competing interest

The authors declare that they have no known competing financial interests or personal relationships that could have appeared to influence the work reported in this paper.

Acknowledgments

The work presented herein has been funded by Abu Dhabi Education Council Award for Research Excellence Program (AARE 2019) through grant number AARE19-213 and by Khalifa University of Science and Technology through Faculty Start-up Award (FSU-2020-20). The authors are thankful to Prof. Cesare Stefanini and Healthcare Engineering Innovation Center (HEIC) at Khalifa University under Award No. RC2-2018–022 for facilitating access to the Biaxial Testing Machine. All authors approved the version of the manuscript to be published.

References

[1] J. Sun, Q. Guan, Y. Liu, J. Leng, Morphing aircraft based on smart materials and structures: A state-of-the-art review, J. Intell. Mater. Syst. Struct. 27 (17) (2016) 2289–2312.
[2] S. Barbarino, O. Bilgen, R.M. Ajaj, M.I. Friswell, D.J. Inman, A review of morphing aircraft, J. Intell. Mater. Syst. Struct. 22 (9) (2011) 823–877.
[3] S. Murugan, M.I. Friswell, Morphing wing flexible skins with curvilinear fiber composites, Compos. Struct. 99 (2013) 69–75.
[4] O. Schorsch, A. Lühring, C. Nagel, R. Pecora, I. Dimino, Polymer based morphing skin for adaptive wings, in: 7th ECCOMAS Thematic Conference on Smart Structures and Materials, 2015, pp. 1–13.
[5] N.M. Ursache, T. Melin, A.T. Isikveren, M.I. Friswell, Technology integration for active poly-morphing winglets development, in: Proceedings of the ASME Conference on Smart Materials, Adaptive Structures and Intelligent Systems, SMASIS2008, Vol. 1, 2008, pp. 775–782.
[6] M.M. Keihl, R.S. Bortolin, B. Sanders, S. Joshi, Z. Tidwell, Mechanical properties of shape memory polymers for morphing aircraft applications, in: Smart Structures and Materials 2005: Industrial and Commercial Applications of Smart Structures Technologies, Vol. 5762, 2005, p. 143.
[7] Y. Li, W. Ge, J. Zhou, Y. Zhang, D. Zhao, Z. Wang, D. Dong, Design and experiment of concentrated flexibility-based variable camber morphing wing, Chin. J. Aeronaut. (2021) 9–11.
[8] P.L. Bishay, C. Aguilar, Parametric study of a composite skin for a twist-morphing wing, Aerospace 8 (9) (2021).
[9] I.K. Kuder, A.F. Arrieta, W.E. Raither, P. Ermanni, Variable stiffness material and structural concepts for morphing applications, Prog. Aerosp. Sci. 63 (2013) 33–55.
[10] C.S. Beaverstock, B.K.S. Woods, J.H.S.M. Fincham, M.I. Friswell, Performance comparison between optimised camber and span for a morphing wing, Aerospace 2 (3) (2015) 524–554.
[11] R.M. Ajaj, E.I.S. Flores, M.I. Friswell, G. Allegri, B.K.S. Woods, A.T. Isikveren, W.G. Dettmer, The zigzag wingbox for a span morphing wing, Aerosp. Sci. Technol. 28 (1) (2013) 364–375.
[12] V.P. Galantai, Design and Analysis of Morphing Wing for Unmanned Aerial Vehicles (Master of Science Thesis), University of Toronto., 2012, pp. 1–75.
[13] M.S. Parancheerivilakkathil, R.M. Ajaj, K.A. Khan, A compliant polymorphing wing for small UAVs, Chin. J. Aeronaut. 33 (10) (2015) 2575–2588.
[14] R.M. Ajaj, M.S. Parancheerivilakkathil, M. Amoozgar, Asapp: A polymorphing wing capable of active span extension and passive pitch, in: AIAA Scitech 2021 Forum, No. January, 2021, pp. 1–19.
[15] D.D. Smith, A.T. Isikveren, R.M. Ajaj, M.I. Friswell, Multidisciplinary design optimization of an active nonplanar polymorphing wing, in: 27th Congress of the International Council of the Aeronautical Sciences 2010, Vol. 1, ICAS 2010, 2010, pp. 529–539.
[16] M.T. Kikuta, Mechanical Properties of Candidate Materials for Morphing Wings, Virginia Polytechnic Institute and State University, 2003, p. 138.
[17] J.N. Kudva, Overview of the DARPA smart wing project, J. Intell. Mater. Syst. Struct. 15 (4) (2004) 261–267.
[18] K.R. Olympio, F. Gandhi, L. Asheghian, J. Kudva, Design of a flexible skin for a shear morphing wing, J. Intell. Mater. Syst. Struct. 21 (17) (2010) 1755–1770.
[19] K.R. Olympio, F. Gandhi, Flexible skins for morphing aircraft using cellular honeycomb cores, J. Intell. Mater. Syst. Struct. 21 (17) (2010) 1719–1735.
[20] R. Olympio, F. Gandhi, Zero Poisson's ratio cellular honeycombs for flex skins undergoing one-dimensional morphing, J. Intell. Mater. Syst. Struct. 21 (17) (2010) 1737–1753.
[21] E.A. Bubert, B.K. Woods, K. Lee, C.S. Kothera, N.M. Wereley, Design and fabrication of a passive 1D morphing aircraft skin, J. Intell. Mater. Syst. Struct. 21 (17) (2010) 1699–1717.
[22] B.K. Woods, M.I. Friswell, The adaptive aspect ratio morphing wing: Design concept and low fidelity skin optimization, Aerosp. Sci. Technol. 42 (2015) 209–217.
[23] M. Kölbl, P. Ermanni, Structural design and analysis of an anisotropic, Bi-axially morphing skin concept, Aerosp. Sci. Technol. 120 (2022) 107292.
[24] R.M. Ajaj, M.I. Friswell, M. Bourchak, W. Harasani, Span morphing using the GNATSpar wing, Aerosp. Sci. Technol. 53 (2016) 38–46.
[25] G. Kofod, The static actuation of dielectric elastomer actuators: how does pre-stretch improve actuation? J. Phys. D Appl. Phys. 41 (21) (2008) 215405.
[26] I. Collins, M. Hossain, W.G. Dettmer, I. Masters, Flexible membrane structures for wave energy harvesting: A review of the developments, materials and computational modelling approaches, Renew. Sustain. Energy Rev. 151 (Novemeber) (2021) 11478.
[27] E.A. Bubert, Highly Extensible Skin for a Variable Wing-Span Morphing Aircraft Utilizing Pneumatic Artificial Muscle Actuation, University of Maryland, 2009, pp. 1–122, (2009).
[28] C. Thill, J. Etches, I. Bond, K. Potter, P. Weaver, Morphing skins, Aeronaut. J. (3216) (2008) 1–23.
[29] P. Lochmatter, G. Kovacs, S. Michel, Characterization of dielectric elastomer actuators based on a hyperelastic film model, Sensors Actuators A 135 (2) (2007) 748–757.
[30] M. Wissler, E. Mazza, Mechanical behavior of an acrylic elastomer used in dielectric elastomer actuators, Sensors Actuators A 134 (2) (2007) 494–504.
[31] R.K. Sahu, K. Patra, Characterisation of tensile behaviour of a dielectric elastomer at large deformation, J. Inst. Eng. (India): Ser. C 95 (3) (2014) 207–212.
[32] M. Hossain, D.K. Vu, P. Steinmann, Experimental study and numerical modelling of VHB 4910 polymer, Comput. Mater. Sci. 59 (2012) 65–74.
[33] R. Kaltseis, C. Keplinger, S.J. Adrian Koh, R. Baumgartner, Y.F. Goh, W.H. Ng, A. Kogler, A. Tröls, C.C. Foo, Z. Suo, S. Bauer, Natural rubber for sustainable high-power electrical energy generation, RSC Adv. 4 (53) (2014) 27905–27913.
[34] A. Helal, M. Doumit, R. Shaheen, Biaxial experimental and analytical characterization of a dielectric elastomer, Appl. Phys. A 124 (1) (2018) 2.
[35] D. Ahmad, K. Patra, Experimental and theoretical analysis of laterally pre-stretched pure shear deformation of dielectric elastomer, Polym. Test. 75 (February) (2019) 291–297.
[36] D. Ahmad, S.K. Sahu, K. Patra, Fracture toughness, hysteresis and stretchability of dielectric elastomers under equibiaxial and biaxial loading, Polym. Test. 79 (2019) 106038.
[37] M. Johlitz, S. Diebels, Characterisation of a polymer using biaxial tension tests. Part I: Hyperelasticity, Arch. Appl. Mech. 81 (10) (2011) 1333–1349.
[38] D. Ahmad, R.M. Ajaj, Multiaxial mechanical characterization of latex skin for morphing wing application, Polym. Test. 106 (2021) 107408, 2021.
[39] X. Li, T. Bai, Z. Li, L. Liu, Influence of the temperature on the hyper-elastic mechanical behavior of carbon black filled natural rubbers, Mech. Mater. 95 (2016) 136–145.
[40] Z. Liao, M. Hossain, X. Yao, R. Navaratne, G. Chagnon, A comprehensive thermo-viscoelastic experimental investigation of Ecoflex polymer, Polym. Test. 86 (March) (2020) 106478.
[41] Libidex Ltd T/A radical rubber, 2022, https://www.radicalrubber.co.uk. (Accessed 11 March 2022).
[42] Oppo medical inc, 2022, https://www.oppomedical.com. (Accessed 11 March 2022).
[43] Smooth-on, 2022, https://www.smooth-on.com. (Accessed 11 March 2022).
[44] A.M. Pankonien, Smart material wing morphing for unmanned aerial vehicles, no. June, 2015, Available: https://deepblue.lib.umich.edu/handle/2027.42/111533.
[45] Z. Liao, X. Yao, L. Zhang, M. Hossain, J. Wang, S. Zang, Temperature and strain rate dependent large tensile deformation and tensile failure behavior of transparent polyurethane at intermediate strain rates, Int. J. Impact Eng. 132 (2019) 12–16.
[46] C. Harvey, L.L. Gamble, C.R. Bolander, D.F. Hunsaker, J.J. Joo, D.J. Inman, A review of avian-inspired morphing for UAV flight control, Prog. Aerosp. Sci. 132 (April) (2022) 100825.
[47] A. Kumar, D. Ahmad, K. Patra, M. Hossain, Enhancement of electromechanical properties of natural rubber by adding barium titanate filler : An electro-mechanical study, J. Appl. Polym. Sci. 138 (February) (2021) 12–16.
[48] Z. Liao, M. Hossain, X. Yao, Ecoflex polymer of different shore hardnesses: Experimental investigations and constitutive modelling, Mech. Mater. 144 (February) (2020).

[49] E.R. Cholleti, J. Stringer, P. Kelly, C. Bowen, K. Aw, The effect of barium titanate ceramic loading on the stress relaxation behavior of barium titanate-silicone elastomer composites, Polym. Eng. Sci. 60 (12) (2020) 3086–3094.
[50] J.S. Bergstrom, M.C. Boyce, Constitutive modeling of the large strain time-dependent behaviour of elastomers, J. Mech. Phys. Solids 46 (5) (1998) 931–954.
[51] S. Lee, M. Pharr, Sideways and stable crack propagation in a silicone elastomer, Proc. Natl. Acad. Sci. USA 116 (19) (2019) 9251–9256.
[52] D. Ahmad, K. Patra, M. Hossain, A. Kumar, Crack propagation behaviour of laterally constrained polymers used as dielectric elastomers, Rubber Chem. Technol. 94 (3) (2021) 476–493.
[53] S. Krpovic, K. Dam-Johansen, A.L. Skov, Importance of mullins effect in commercial silicone elastomer formulations for soft robotics, J. Appl. Polym. Sci. 138 (19) (2021) 1–15.
[54] Z. Liao, M. Hossain, X. Yao, R. Navaratne, G. Chagnon, A comprehensive thermo-viscoelastic experimental investigation of Ecoflex polymer, Polym. Test. 86 (March) (2020) 106478.
[55] M. Pharr, J.Y. Sun, Z. Suo, Rupture of a highly stretchable acrylic dielectric elastomer, J. Appl. Phys. 111 (10) (2012) 104114.
[56] T.T. Mai, K. Okuno, K. Tsunoda, K. Urayama, Anisotropic stress-softening effect on fast dynamic crack in filler-reinforced elastomers, Mech. Mater. 155 (2021) 103786.
[57] R.D. Vocke, C.S. Kothera, B.K. Woods, N.M. Wereley, Development and testing of a span-extending morphing wing, J. Intell. Mater. Syst. Struct. 22 (9) (2011) 879–890.